Scattering from Dielectric Mirrors

By D. GLOGE, E. L. CHINNOCK, and H. E. EARL

(Manuscript received September 9, 1968)

Most of the light scattered from high-reflectivity dielectric mirrors is radiated into directions close to the reflected beam. We measured the angular power distribution at angles between 0.01° and 1° from the beam axis by scanning with a narrow slit. From this a linear structure function is calculated for coherence lengths between 20 microns and 1 millimeter, assuming isotropic surface statistics. The corresponding power density decreases with the third power of the scattering angle. The power outside a given radius and the power density is plotted for various wavelengths and distances.

I. INTRODUCTION

The improvement of dielectric mirrors during recent years has reduced their surface scattering considerably. Nevertheless, there are applications which are limited by these small amounts of scattered light. One of them is the laser gyroscope whose locking threshold depends on the light scattered back into the direction of incidence. Measurements have been performed recently to analyze this case.[1]

Another application is the simultaneous transmission of many laser beams in an optical waveguide for communication purposes.[2] The focusers in such a guide will probably be front surface mirrors rather than lenses because, for the large apertures needed, lenses are apt to have imperfections in the bulk. Dielectric mirrors have fewer imperfections, but they still scatter some light into adjacent beams where it produces crosstalk. It was the purpose of our experiment to measure some representative mirror surfaces as a basis for later feasibility studies on multiple beam waveguides. Only the light in a narrow cone around the beam is collected by the next focuser and eventually contributes to the crosstalk. The experiment showed that, in this cone, the scattered light intensity decreases relatively fast with increasing angle.

Applying these results to more complicated problems requires a simple but adequate mathematical representation of the results. We found that the standard scattering theory, which uses a covariance function to describe the mirror surface statistics, serves this purpose very poorly.[3] On the other hand, a simple structure function can be found which is a satisfactory representation of the physical reality in the range of the measurements and is easily applicable to practical problems.

II. SCANNING THE SCATTERED POWER DISTRIBUTION

The measurements were performed with a 50-cm He-Ne laser generating a 1-milliwatt gaussian beam at 6328Å. To achieve enough sensitivity and discrimination against noise, the laser beam was chopped for signal processing in a lock-in amplifier as shown in Fig. 1.

A slit was used to scan the scattered light. This requires scanning only in one direction (while the slit averages over the perpendicular coordinate) and more signal power is collected than with a pinhole method. Because of its circular symmetry, the scattered power density can be calculated from this measurement by a simple integral transformation.

To avoid scattering from dust particles in the beam path to and from the mirror, this path was evacuated to about 4 torr. But careful comparison with measurements in unfiltered, though quiet, air showed no measureable difference.

The mirror had a radius of curvature of 24 m and a diameter of 15 cm. The beam, having a $1/e$-width of 24 mm at the mirror, was focused to 0.8 mm in the plane of the slit. The slit was 0.15 mm wide. Figure 2 shows the relative intensities normalized to the peak

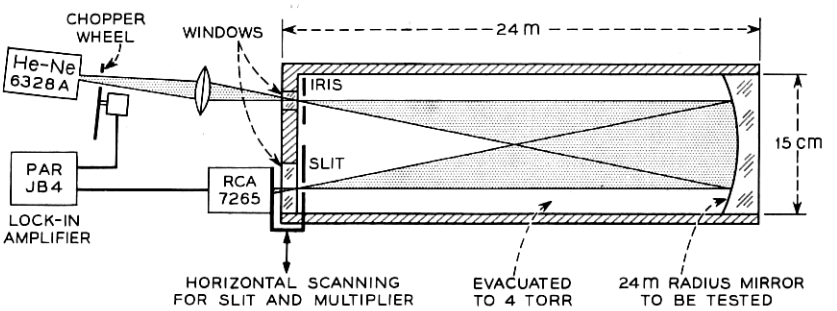

Fig. 1 — Setup to measure the scattering under vacuum.

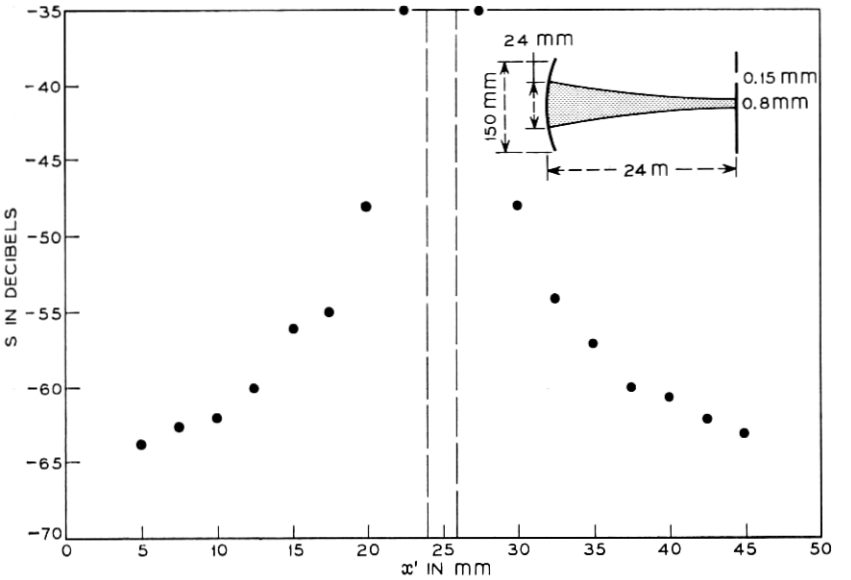

Fig. 2 — Scattered power at 24-m distance normalized to the peak power (the vertical lines are part of the coherent beam profile).

intensity in dB and plotted versus the vertical coordinate. In this logarithmic plot, the gaussian intensity profile of the coherent signal has a parabolic shape, part of which is represented by the almost vertical lines in the center of Fig. 2. If diffraction and spherical aberrations are taken into consideration, the fall-off is not quite as sharp as indicated by the parabola, but these effects were estimated to be well below the light levels measured. Therefore, we believe that surface scattering is the sole source for our results. The scanning range in Fig. 2 corresponds to angles from 0.01 to 0.1 degree.

For larger angles up to 1 degree, a 1-m set-up was used which was basically similar to the one shown in Fig. 1, but had no vacuum enclosure. The five mirrors tested in this arrangement had a radius of curvature of 1 m, a diameter of 25 mm, and the same coating as the 24-m mirror. The test beam in this set-up was 4 mm wide at the mirror and was focused to 0.2 mm at the slit. The slit had a width of 0.05 mm. Coatings from different batches showed up to 3 dB difference. Figure 3 shows average and variation of the results. Again the intensity normalized to the peak intensity is plotted in dB. The profile of the coherent beam is shown in the center.

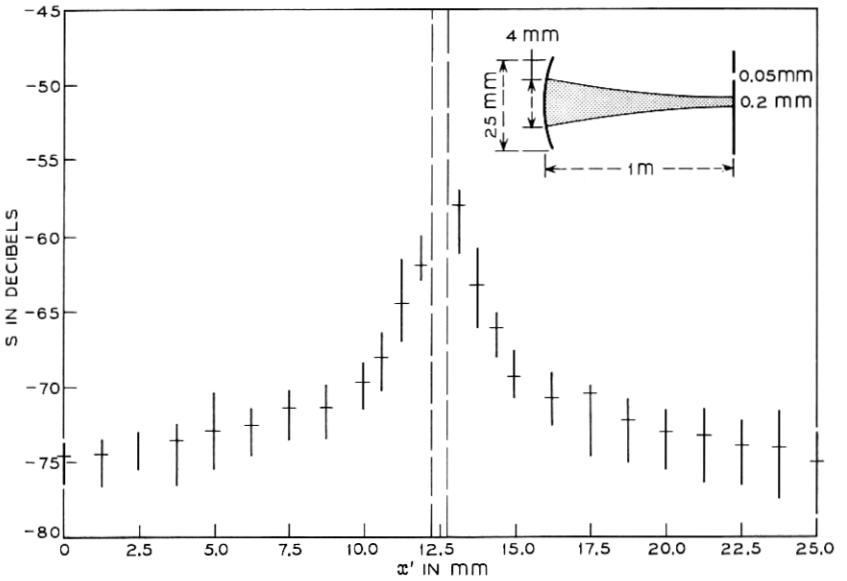

Fig. 3 — Scattered power at 1-m distance normalized to the peak power (the vertical lines are part of the coherent beam profile).

Both the 24-m mirror and the 1-m mirror were polished and coated by the same methods though by different manufacturers. They were tested to be spherical within $\lambda/10$. The reflection loss of the 24-m mirror was measured by a multiple reflection technique to be 0.135%. The mirrors were measured new without previous use, but no increase of the scattering was measured by repeated checks during the following weeks. Further lifetime studies are under way.

III. DESCRIPTION OF THE SCATTERING SURFACE

The scattering plotted in Figs. 2 and 3 originates from a slight roughness or ripple structure $\delta(X, Y)$ on the mirror surfaces which is, of course, different for different mirrors. The surfaces tested in this experiment, however, were manufactured by the same process and are therefore equivalent in a statistical sense. That implies that the average magnitude of each ripple component, that is, the "power spectrum" of $\delta(X, Y)$, is the same from mirror to mirror. The average has to be taken over an ensemble of test surfaces; however, for correlation lengths small compared to the test area, the ensemble average

may be replaced by an average over the individual surface. In this case, measuring only one or a few surfaces still yields a meaningful result, though only for correlation lengths small compared to the radius w of the light beam at the mirror surface.

The "power spectrum" is closely related to the scattering profile measured by the slit method. A vertical slit at X', as in Fig. 4, collects mainly light scattered from the vertical ripple component with the spatial frequency

$$x = \frac{X'}{L\lambda} \tag{1}$$

where λ is the light wavelength and L the distance between slit plane and mirror. Therefore, apart from a constant, the scattered profile $s(X')$ of Figs. 2 and 3 agrees with the "power spectrum" $d_x(x)$ of $\delta(X, Y)$ for Y = constant.* The quantitative relation between d_x and s is given in (38) of Appendix A and reads

$$d_x(x) = \frac{L\lambda^3}{16\pi^2 t} \operatorname{erf}\left(\frac{\pi w t}{\sqrt{2}\,\lambda L}\right) s(x). \tag{2}$$

where t is the slit width and w the $1/e$-width of the gaussian light beam at the mirror surface. A log-log plot of $d_x(x)$ is shown in Fig. 5. The points on the left hand side are taken from Fig. 2 and represent the 24-m experiment, the ones on the right hand side stem from Fig. 3 and the 1-m experiment. Since the mirrors are statistically equivalent, all these points belong to the same function. A rough approximation is attempted by the straight line in Fig. 5 which represents the function

$$d_x(x) = \frac{D}{x^2} \tag{3}$$

with

$$D = 6 \cdot 10^{-14} \text{ mm}. \tag{4}$$

The Fourier transform of d_x is the covariance of $\delta(X, Y)$ along lines Y = constant.[3] It proves impossible, however, to perform this transform without knowing d_x for very small x where it increases rapidly. Accurate information about this range is unnecessary if the

* Strictly speaking, $s(x)$ is a two-fold convolution of $d_x(x)$ with the intensity profile of the beam and the slit aperture function; but because the latter two functions are very narrow as compared to the scattered profile, the above simplification is appropriate.

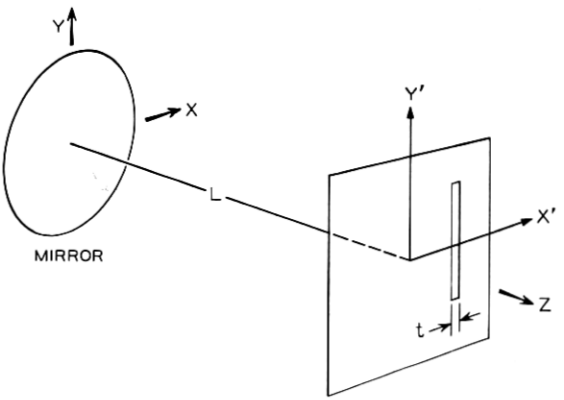

Fig. 4 — Sketch of the experiment showing the coordinate system used.

structure function

$$\Delta(X_1 - X_2\,,\ Y_1 - Y_2) = \langle[\delta(X_1\,,\ Y_1) - \delta(X_2\,,\ Y_2)]^2\rangle_{av} \qquad (5)$$

is used instead. The interrelation between Δ and d_x is derived in the Appendix A and given in (39). It involves the transformation

$$\int_0^\infty d_x(x) \sin^2 (\pi X x)\, dx.$$

The $\sin^2$-kernel of this transformation reduces the contribution from the zero-end of the d_x-function and $\Delta(X, 0)$ can therefore be calculated more accurately in the range of interest than the covariance.

Inserting (3) into (39) yields the functional approximation

$$\Delta(X, 0) = -\frac{\lambda^2}{8\pi^2}\left[\frac{1}{2}\frac{X^2}{w^2} + \ln\left(1 - \frac{32\pi^4}{\lambda^2} DX\right)\right], \qquad (6)$$

where X has the meaning of a correlation length. In the range $X < w$, which is shown in Fig. 6, the structure function (6) is essentially a straight line given by

$$\Delta(X, 0) = 4\pi^2 DX. \qquad (7)$$

This result suggests that the mean square difference between samples of δ increases proportionally to the distance at which they are taken. At the right side of Fig. 6 the quantity $(\Delta)^{1/2}$ can be read off, which indicates a direct measure of the heights of the surface irregularities as a function of their extension about the surface. This

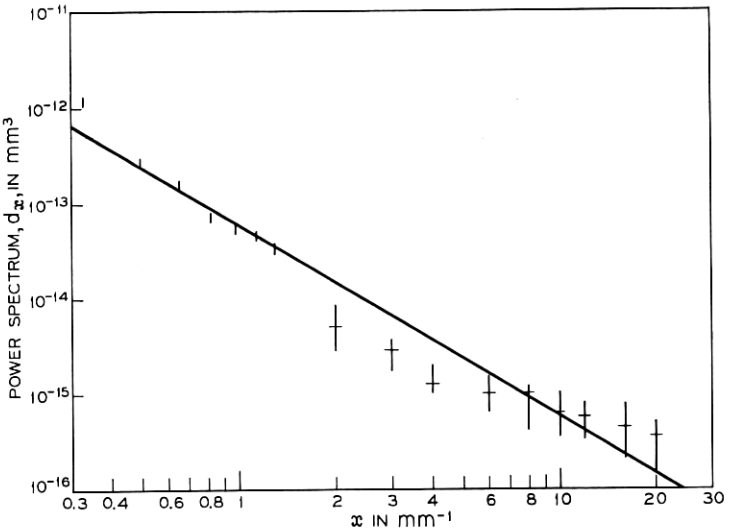

Fig. 5 — Power spectrum of the mirror surface roughness. The line represents a best-fit approximation to the measured points.

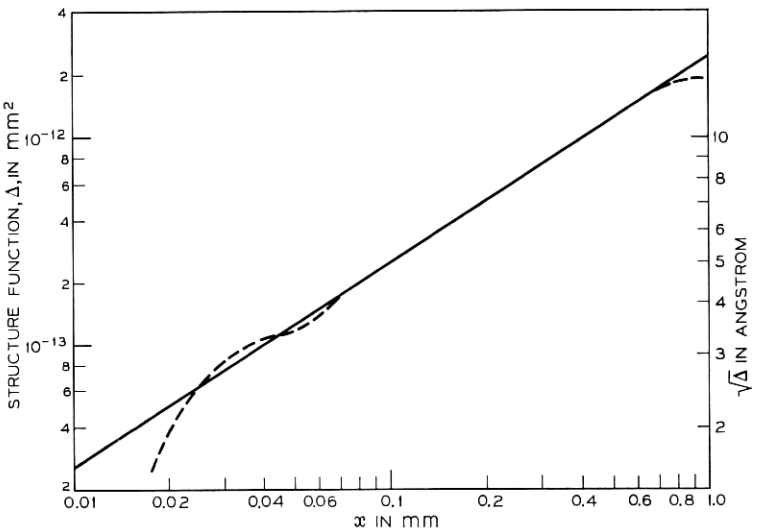

Fig. 6 — The structure function Δ calculated from the approximated power spectrum. The broken line indicates the possible uncertainty of the result.

quantity does not, at least not in the measured interval, approach a definite rms value, but increases unlimited for larger and large sampling distances. This is not necessarily in contrast to physical reality, but one has to keep in mind that, for macroscopic sampling distances, the statistics of δ are probably governed by a different process, which could mean a steeper rise as well as a leveling off for the structure function.

Unknown contributions from outside the measured interval of d_x will to some degree affect the accuracy with which (7) can be evaluated. Ruling out any poles of d_x for $x \neq 0$ (which would mean nonstatistical components), a "worst case" may be established by assuming that (3) holds only in the measured interval $x_1 < x < x_2$, everywhere else $d_x(x) = 0$. Then from (39) with $x \ll w$ and $\Delta \ll 1$

$$\Delta(X, 0) = 8D \int_{x_1}^{x_2} \frac{\sin^2 (\pi X x)}{x^2} \, dx \tag{8}$$

with $x_1 = 0.3\text{mm}^{-1}$ and $x_2 = 30\text{mm}^{-1}$. The dashed line in Fig. 6 shows the evaluation of this integral. The accuracy seems satisfactory for coherence lengths between 20μ and 1 mm.

Though $\Delta(X, 0)$ describes the statistics of δ only along lines $Y =$ constant, this result can easily be generalized assuming that the mirror surface is isotropic. Then the structure function has circular symmetry and can be expressed as a function of the radius $R = (X + Y^2)^{1/2}$. This function reads

$$\Delta(R) = \Delta(R, 0) \tag{9}$$

where $\Delta(R, 0)$ is given by (7).

IV. THE DISTRIBUTION OF THE SCATTERED POWER

For most applications the actual scattered light distribution around the beam is of more immediate interest than the structure function. Of course, this light distribution not only depends on the properties of the mirror, but also on the properties of the light beam reflected off the mirror. More specifically, this light distribution is the convolution of the intensity profile of the primary beam with the "power spectrum" of the mirror irregularities. Only when the beam profile is very narrow, as in our experiment, do the scattered light distribution and the "power spectrum" become proportional functions.

In this section we evaluate this distribution for various optical wavelengths in arbitrary cross sections of the beam. If applied to

problems where the width of the beam may not be neglected, the convolution of this function with the intensity profile of the beam has to be formed.

Because of the isotropy of the mirror surface, the scattering has circular symmetry. If we define a normalized radius $r = (x^2 + y^2)^{1/2}$, the scattered light distribution $p(r)$ can be calculated from (32) of Appendix A. By substituting x by r in (32), one obtains

$$S(x) = \frac{2t}{L\lambda} \int_x^\infty \frac{p(r) r \, dr}{(r^2 - x^2)^{1/2}}, \tag{10}$$

where r is related to the radius $R' = (X'^2 + Y'^2)^{1/2}$ by the normalization

$$r = \frac{R'}{L\lambda}. \tag{11}$$

One can solve (10) for $p(r)$ by multiplying both sides by $x dx/(x^2 - r^2)^{1/2}$ and integrating with respect to x from r to ∞.[4] After interchanging the order of integration on the right-hand side, the integral over x can be evaluated and one obtains

$$\frac{L\lambda}{2t} \int_r^\infty \frac{x S(x) \, dx}{(x^2 - r^2)^{1/2}} = \int_r^\infty 2\pi r p(r) \, dr. \tag{12}$$

The integral on the right represents the total power scattered outside a circle with radius r and will be called $P(r)$ in the following. Insertion of (2), (27), and (35) into (12) yields

$$P(r) = P_{tot} \frac{8\pi^2}{\lambda^2} \int_r^\infty \frac{x d_x(x) \, dx}{(x^2 - r^2)^{1/2}}; \tag{13}$$

and the power density $p(r)$ is finally obtained from the differentiation

$$p(r) = -\frac{1}{2\pi r} \frac{dP}{dr}. \tag{14}$$

By using (3) for d_x in (13), one obtains for the power outside the radius r

$$P(r) = \frac{4\pi^3}{\lambda^2} \frac{D}{r} P_{tot} \tag{15}$$

and the power density

$$p(r) = \frac{2\pi^2}{\lambda^2} \frac{D}{r^3} P_{tot}. \tag{16}$$

To gain information about the power density as a function of the scattering direction, one may multiply (11) by λ and find the scattering angle

$$\rho = \lambda r = \frac{R'}{L}. \tag{17}$$

The power scattered into directions deviating by more than ρ from the beam axis is obtained by inserting (17) into (15)

$$P\left(\frac{\rho}{\lambda}\right) = \frac{4\pi^3}{\lambda}\frac{D}{\rho}P_{tot}\,. \tag{18}$$

The derivative with respect to ρ yields the angular power density

$$p_\rho(\rho) = -\frac{1}{2\pi\rho}\frac{dP}{d\rho} = \frac{2\pi^2}{\lambda}\frac{D}{\rho^3}P_{tot}\,. \tag{19}$$

Equations (18) and (19) are evaluated for various wavelengths in Figs. 7 and 8. Figure 7 shows the power fraction outside ρ which decreases linearly with increasing radius. Fig. 8 shows the power fraction radiated into a given solid angle at ρ. This function decreases with the third power of ρ.

Finally, for a certain distance L, one finds the power arriving out-

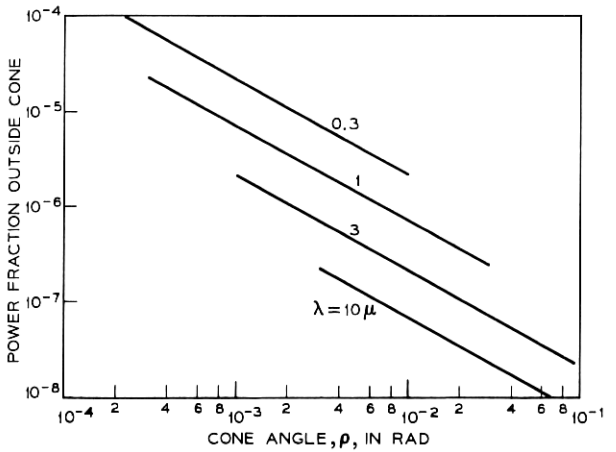

Fig. 7 — The total power fraction scattered with an angle larger than ρ off the beam axis for various wavelengths λ.

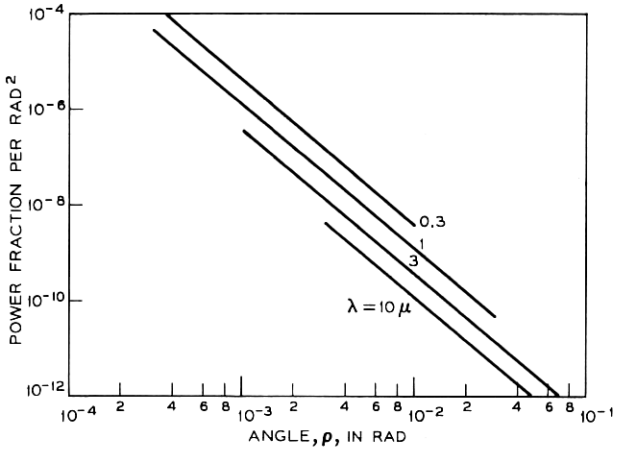

Fig. 8 — The angular power density as a function of the scattering angle ρ for various wavelengths λ.

side a circle of radius R' to be

$$P\left(\frac{R'}{L\lambda}\right) = 4\pi^3 \frac{DL}{\lambda R'} P_{tot} \tag{20}$$

and the derivative with respect to R' yields

$$p_{R'}(R') = -\frac{1}{2\pi R'} \frac{dP}{dR'} = 2\pi^2 \frac{DL}{\lambda R'^3} P_{tot} , \tag{21}$$

where $p_{R'}$ is the scattered power density at a distance L. Equation (20) is plotted for various L in Fig. 9. Figure 10 shows the power density versus the radius which decreases with the third power of R'. It is interesting that the power density at a fixed radius increases proportional to the distance from the scatterer.

Of course, equations (15) through (21) hold only for $r < 0.3$ mm^{-1}, the lower limit of the interval measured, and are based on the assumption that (3) is valid for $r > 30$ mm^{-1}. However, as d_x is small in the latter region, a possible error introduced by this assumption should not be significant in the range of interest.

V. CONCLUSIONS

The small angle scattering was measured for very highly reflecting dielectric mirrors. A reasonable functional approximation for the

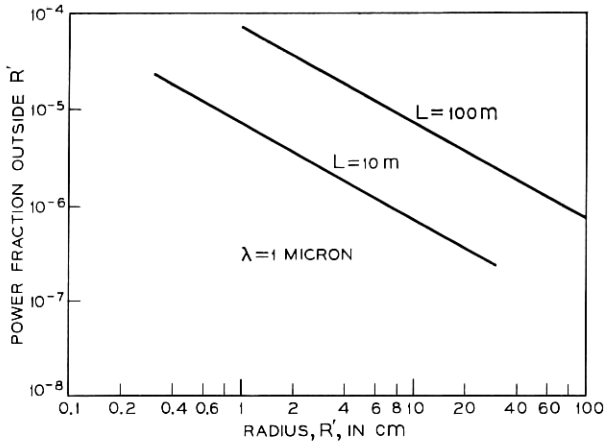

Fig. 9 — The total power fraction scattered outside a circle with radius R' at various distances L.

measurements leads to a linear structure function for coherence lengths between 20 microns and 1 mm. The rms difference between surface deviations found at two points 1 mm apart is 30 Angstroms and decreases with the root of the distance for points closer together. At an angle of 0.1° the scattered power density per cm² is 10^{-6} of the total power. It decreases proportional to the third power of the angle

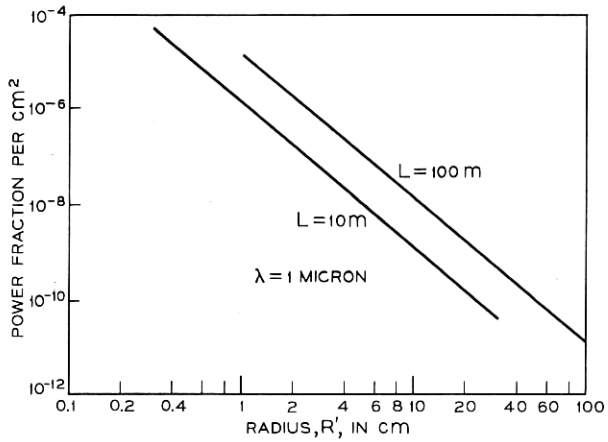

Fig. 10 — The scattered power density as a function of the radius R' at various distances L.

and linearly with the light wavelength. No considerable differences were found for mirrors polished and coated by two different manufacturers which were using the same processes and chemicals.

VI. ACKNOWLEDGMENTS

We are thankful for stimulating discussions and fruitful suggestions by H. E. Rowe and E. A. J. Marcatili.

APPENDIX

The Structure Function

Consider a coherent Gaussian beam of wavelength λ to be reflected off the mirror in Fig. 4 and focused on a plane with a slit. Assume that unperturbed phase fronts emanating from the mirror were spherical with a field distribution

$$E(X, Y) = E_0 \exp [-(X^2 + Y^2)/w^2]. \tag{22}$$

The mirror diameter may be considered sufficiently large compared to the $1/e$-width w so that the field at the mirror edge may be neglected. In this case, the field in the focal plane is

$$f(x, y) = \iint_{-\infty}^{+\infty} e^{-i2\pi(Xx+Yy)} E(X, Y)\, dX\, dY \tag{23}$$

where

$$x = \frac{X'}{L\lambda} \quad \text{and} \quad y = \frac{Y'}{L\lambda} \tag{24}$$

are the normalized coordinates in the focal plane (see Fig. 4). The solution of (23) is

$$f(x, y) = E_0 w^2 \pi \exp [-\pi^2 w^2 (x^2 + y^2)]. \tag{25}$$

The total power

$$P_{tot} = \frac{\pi w^2}{2} E_0^2 \tag{26}$$

can be calculated by integrating (22) or (25).

Assume that the slit in the focal plane is long enough to collect all the power in y-direction and has a width t in x-direction. Then for $X' = 0$ the signal received is

$$S(0) = P_{tot} \operatorname{erf}\left(\frac{\pi w t}{\sqrt{2}\, L\lambda}\right) \tag{27}$$

where erf denotes the error function. This is the peak signal measured with no scattering present. However, for the case in question where the scattered power is less than a percent, (27) can also be used for the peak center signal of the scattering profile.

The scattering under consideration originates from a slight roughness $\delta(X, Y)$ of the mirror surface which gives rise to a phase variation

$$\varphi(X, Y) = \frac{4\pi}{\lambda} \delta(X, Y) \tag{28}$$

on the otherwise perfect phase front. The term $\delta(X, Y)$ is assumed to be a gaussian random process with isotropic statistics. Its structure function is given by (5).

It can be shown that for gaussian statistics[5]

$$\langle \exp i[\varphi(X_0 , Y_1) - \varphi(X_2 , Y_2)] \rangle = \exp\left[-\frac{8\pi^2}{\lambda^2} \Delta\right]. \tag{29}$$

The power density in the focal plane can be calculated from (23) by introducing the phase factor $\exp[-i\varphi(X, Y)]$ and then multiplying (23) by its conjugate complex. Using (29) yields finally

$$\begin{aligned} p(x, y) = \iiiint_{-\infty}^{+\infty} & E(X_1 , Y_1)E(X_2 , Y_2) \\ & \cdot \exp\left[-\frac{8\pi^2}{\lambda^2} \Delta(X_1 - X_2 , Y_1 - Y_2)\right] \\ & \cdot \exp\left[-i2\pi(X_1 - X_2)x\right] \\ & \cdot \exp\left[-i2\pi(Y_1 - Y_2)y\right] dX \; dX_2 \, dY_1 \, dY_2 . \end{aligned} \tag{30}$$

After a standard coordinate transformation, this becomes

$$\begin{aligned} p(x, y) = P_{tot} \iint_{-\infty}^{+\infty} & \exp\left[-(X^2 + Y^2)/2w^2\right] \\ & \cdot \exp\left[-\frac{8\pi^2}{\lambda^2} \Delta(X, Y)\right] \exp\left[-i2\pi(Xx + Yy)\right] dX \, dY. \end{aligned} \tag{31}$$

To measure the relatively flat power distribution outside the coherent beam, one may average over the slit width t and consequently the signal measured in this region is approximately

$$S(x) = \frac{t}{L\lambda} \int_{-\infty}^{+\infty} p(x, y) \, dy. \tag{32}$$

Because of (31), this becomes

$$S(x) = \frac{t}{L\lambda} P_{tot} \int_{-\infty}^{+\infty} \exp\left[-\frac{1}{2}\frac{X^2}{w^2} - \frac{8\pi^2}{\lambda^2}\Delta(X, 0)\right] e^{-i2\pi Xx}\, dX. \quad (33)$$

For experimental convenience the normalized signal

$$s(x) = \frac{S(x)}{S(0)} \quad (34)$$

was measured and plotted in Figs. 2 and 3. From (27) and (33) one finds

$$s(x) = \frac{t}{L\lambda}\left[\operatorname{erf}\left(\frac{\pi wt}{\sqrt{2}\, L\lambda}\right)\right]^{-1} \cdot \int_{-\infty}^{+\infty} \exp\left[-\frac{1}{2}\frac{X^2}{w^2} - \frac{8\pi^2}{\lambda^2}\Delta(X, 0)\right] e^{-i2\pi Xx}\, dX. \quad (35)$$

Inverting the Fourier transformation in (35) yields

$$\exp\left[-\frac{1}{2}\frac{X^2}{w^2} - \frac{8\pi^2}{\lambda^2}\Delta(X, 0)\right] = \frac{L\lambda}{t} \operatorname{erf}\left(\frac{\pi wt}{\sqrt{2}\, L\lambda}\right) \int_{-\infty}^{+\infty} s(x) e^{i2\pi Xx}\, dx. \quad (36)$$

The evaluation of this integral is problematic for small x where the measurements are impeded by the coherent beam, but where $s(x)$ is large and contributes significantly to the dc component of $\Delta(X, 0)$. To overcome this difficulty, the identity $\Delta(0, 0) = 0$ can be used which is based on the definition (5) of the structure function. Incorporating this identity (36) can be rewritten in the form

$$1 - \exp\left[-\frac{1}{2}\frac{X^2}{w^2} - \frac{8\pi^2}{\lambda^2}\Delta(X, 0)\right] = \frac{L\lambda}{t} \operatorname{erf}\left(\frac{\pi wt}{\sqrt{2}\, \lambda L}\right) \int_{-\infty}^{+\infty} s(x)[1 - e^{i2\pi Xx}]\, dx. \quad (37)$$

The function

$$d_x(x) = \frac{L\lambda^3}{16\pi^2 t} \operatorname{erf}\left(\frac{\pi wt}{\sqrt{2}\, \lambda L}\right) s(x) \quad (38)$$

may be interpreted as the "power spectrum" of $\delta(X, Y)$ for $Y =$ constant. Consequently, x has the meaning of a spatial frequency related to the Fourier components of δ along lines $Y =$ constant. d_x

as well as s are even functions of x. Therefore, the solution for $\Delta(X, 0)$ can be written in the form

$$\Delta(X, 0) = \frac{\lambda^2}{8\pi^2}\left\{-\frac{1}{2}\frac{X^2}{w^2} - \ln\left[1 - \frac{64\pi^2}{\lambda^2}\int_0^\infty d_x(x)\sin^2(\pi X x)\,dx\right]\right\}. \tag{39}$$

REFERENCES

1. Beatey, R., "Light Scattering by Laser Mirrors," Appl. Opt., *6*, No. 5 (May 1967), pp. 831–835.
2. Gloge, D., and Weiner, D., "The Capacity of Multiple Beam Transmission Systems and Optical Delay Lines," B.S.T.J., *47*, No. 10 (December 1968), pp. 2095–2109.
3. Beckmann, P. and Spizzichino, A., *The Scattering of Electromagnetic Waves from Rough Surfaces*, New York: Pergamon Press, 1963.
4. Harker, K. J., "Use of Scanning Slits for Obtaining the Current Distribution in Electron Beams," J. Appl. Phys., *28*, No. 11 (November 1957), pp. 1354–1357.
5. O'Neill, E. L., *Introduction to Statistical Optics*. New York: Addison-Wesley Publishing Co., 1963, p. 100.